tions can be decreased by reducing the time step or lowering the maximum shear mixing coefficient (ν_o^{sh}), but neither solution is satisfactory in general. Limiting the time step to the degree necessary to prevent the oscillations can become prohibitively expensive for three-dimensional calculations. Reducing ν_o weakens the mixing produced by the scheme everywhere that the shear mechanism is active. Thus model resolution must be carefully chosen.

[61] A further complication to these issues for the coastal ocean is the common use of terrain-following coordinate systems. A typical domain can range from 15 cm vertical resolution at the coastal boundary to 10 m resolution offshore. In such a setting, spatial gradients in mixing can develop because of these numerical issues alone. The most promising solution to these issues would seem to lie in finding an alternative to the Richardson number based approach for the interior.

5. Interacting Surface and Bottom Boundary Layers: Case 2

[62] Next the vertical mixing in a one-dimensional water column in which surface and bottom boundary layers are in close proximity is examined. In these experiments both stratification and water depth are varied. The wind forcing leads to the deepening of the surface boundary layers as in case 1, but because of the constraint of zero net horizontal transport, a bottom boundary layer in which the flow is reversed also forms. In all sensitivity studies the response of the bottom boundary layer was observed to be analogous to that of the surface one. That is, while the two boundary layers were not close enough to be affecting each other (greater than approximately 1 m of stratified water between them), the entrainment and deepening of each followed the patterns observed for case 1. The bottom boundary layer produced by M-Y entrained more and extended higher than KPP in strong stratification, and less when the vertical density gradient was low. At the highest initial stratification examined (N_o), the surface and bottom boundary layers remained separated by several meters of strong stratification for the duration of the simulations for all water depths considered. For weaker vertical density gradients interaction between the boundary layers was observed.

[63] Figure 13 depicts time-depth contour plots for simulations with $N_o/10$ stratification in water depths of 15, 17, 18, and 20 m. At 20 m water depth the basic behavior of case 1 can be observed. There is greater deepening and entrainment with the Mellor-Yamada scheme into both the surface and bottom boundary layers. By day six the stratification in the pycnocline has intensified significantly to approximately 6 times the initial value. For shallower water depths, under the same forcing conditions the response gradually changes particularly with the M-Y scheme. The intensified pycnocline that develops between the boundary layers gradually moves upward with the M-Y parameterization but not with KPP. This process reduces the depth of the surface boundary layer while increasing the height of the bottom boundary layer. While the KPP simulations for these water depths show slower growth of the boundary layers and, consequently, less interaction, there is no indication even in the 15 m depth simulation that the pycnocline will move upward when the top and bottom turbulent regions come in close proximity.

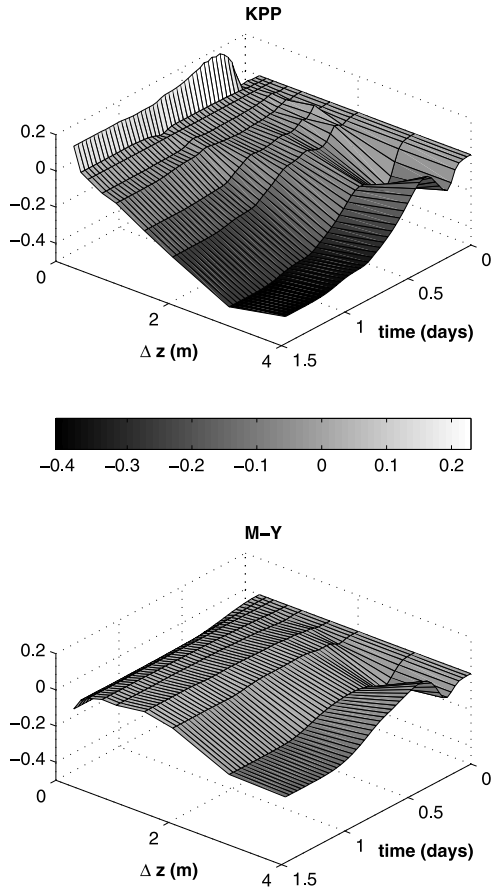

Figure 12. Surface plots displaying the sensitivity of the two parameterizations to vertical grid resolution. The vertical axis shows percent deviation of the surface density field relative to the base (50 cm vertical resolution) case.

[64] The shallowing of the pycnocline with the Mellor-Yamada scheme occurs because the tendency of the bottom boundary layer to grow exceeds that of the surface boundary layer. The gradient in the mixing coefficient at the top of the bottom boundary layer forces the stratification to intensify in the pycnocline to an extent such that at the bottom of the surface boundary layer

$$\frac{\partial K_\rho}{\partial z}\frac{\partial \rho}{\partial z} < K_\rho \frac{\partial^2 \rho}{\partial z^2}. \tag{31}$$

This results in a net upward flux of density. Figure 14 shows profiles of the vertical mixing coefficient for the two schemes for the 15 and 18 m water depth $N_o/10$ simulations. In M-Y the strong upward movement of the pycnocline in the 15 m case can be compared to the negligible movement in the 18 m case (Figure 14). For the shallower water column the bottom boundary layer is confined to a thinner layer. Velocity shears at the top of the boundary layer are higher and turbulent kinetic energy production is enhanced. This results in a stronger - $\partial_z K_\rho$ at the top of the bottom boundary layer than at the bottom of the surface one. For a water column just 3 m deeper the